Translational Oncology 13 (2020) 100760

Contents lists available at ScienceDirect

Translational Oncology

journal homepage: www.elsevier.com/locate/tranon

Modulating the Distant Spreading of Patient-Derived Colorectal Cancer Cells via Aspirin and Metformin

Gemma Palazzolo [a,*], Hilaria Mollica [a], Valeria Lusi [a], Mariangela Rutigliani [b], Martina Di Francesco [a], Rui Cruz Pereira [a,1], Marco Filauro [c], Laura Paleari [d,2], Andrea DeCensi [e,2], Paolo Decuzzi [a,2]

[a] Laboratory of Nanotechnology for Precision Medicine, Fondazione Istituto Italiano di Tecnologia, 16163 Genoa, Italy
[b] Department of Laboratory and Service, Histological and Anatomical Pathology Unit, E.O. Ospedali Galliera, Genoa, Italy
[c] Department of Surgery, E.O. Ospedali Galliera, Genoa, Italy
[d] ALiSa, Liguria Health Authority, Genoa, Italy
[e] Department of Medicine Area, Medical Oncology Unit, E.O. Ospedali Galliera, Genoa, Italy

ARTICLE INFO

Article history:
Received 12 February 2020
Received in revised form 9 March 2020
Accepted 11 March 2020
Available online xxxx

ABSTRACT

Although screening has reduced mortality rates for colorectal cancer (CRC), about 20% of patients still carry metastases at diagnosis. Postsurgery chemotherapy is toxic and induces drug resistance. Promising alternative strategies rely on repurposing drugs such as aspirin (ASA) and metformin (MET). Here, tumor spheroids were generated in suspension by primary CRCs and metastatic lymph nodes from 11 patients. These spheroids presented a heterogeneous cell population including a small core of $CD133^+/ESA^+$ cancer stem cells surrounded by a thick corona of $CDX2^+/CK20^+$ CRC cells, thus maintaining the molecular hallmarks of the tumor source. Spheroids were exposed to ASA and/or MET at different doses for up to 7 days to assess cell growth, migration, and adhesion in three-dimensional assays. While ASA at 5 mM was always sufficient to mitigate cell migration, the response to MET was patient specific. Only in MET-sensitive spheroids, the 5 mM ASA/MET combination showed an effect. Interestingly, CRCs from diabetic patients daily pretreated with MET gave a very low spheroid yield due to reduced cancer cell survival. This study highlights the potential of ASA/MET treatments to modulate CRC spreading.

Introduction

Colorectal cancer (CRC) is the third cause of cancer-related death worldwide and the second cause in Europe [1]. About 50% of CRC patients die of cancer [2], and half of them are diagnosed when they already carry metastases [3]. Despite growing efforts in predicting the occurrence of CRC [4], identifying new molecular targets [5], and designing novel therapies [6], the major cause of death continues to be related to the onset and proliferation of distant organ metastasis [7]. Although adjuvant chemotherapeutic agents are improving the prognosis for patients with metastatic CRC, the median overall survival (OS) does not exceed 30 months [8]. Hence, there is an urgent medical need for tackling CRC metastasis in order to improve the overall outcome of the therapy and extend patient survival [9]. Given the heterogeneous nature of CRC, including the involvement of diverse patient-specific factors at the molecular scale [10] and the development of intratumor heterogeneity [11], current therapeutic interventions cannot address successfully all patients. Thus, researchers are focusing into untangling both interpatient and intratumor heterogeneity to identify more personalized therapies for preventing tumor recurrence and metastasis.

After resecting the primary cancer, patients with high-risk stage II or stage III CRC would undergo treatment with adjuvant chemotherapeutics in order to hinder, or at least mitigate, the metastatic spread. The standard treatments are typically accompanied by targeted therapies with antibodies against VEGFR [12,13] or EGFR in RAS wild-type tumors [14]. Unfortunately, these combination therapies are highly toxic and quite expensive [15,16]. In addition, CRC patients may often not respond to such therapies because they suffer from either innate or acquired multidrug resistance [17]. To overcome these limitations, researchers are seeking for new biomarkers to develop novel drug molecules as well as repurposing well-known therapeutic agents for CRC treatment.

Aspirin (ASA) and metformin (MET) have a wide and diverse spectrum of pharmacological activities. ASA is well known for its anti-inflammatory potential resulting from the inhibition of COX1 and COX2 [18], whereas MET is an antidiabetic drug affecting insulin sensitivity [19]. Recently, ASA and MET have been also considered for their potential anticancer activities [20–23]. Specifically, the daily administration of low dose of ASA has been associated with a decrease in CRC occurrence and mortality, suggesting a potential dual antitumor effect on cancer incidence and

* Corresponding author at: Enhanced Regenerative Medicine, Fondazione Istituto Italiano di Tecnologia, Via Morego 30, 16163 Genoa, Italy.
E-mail address: gemma.palazzolo@iit.it. (G. Palazzolo).
[1] Current affiliation: Neurobiology of miRNA, Fondazione Istituto Italiano di Tecnologia, 16163 Genoa, Italy.
[2] These authors share senior authorship.

http://dx.doi.org/10.1016/j.tranon.2020.100760

metastases [24–26]. Moreover, ASA has been shown to be well tolerated by patients in adjuvant anticancer therapies [27]. Similarly, MET has been shown to be mostly effective in CRC patients with diabetes [28, 29], and it was documented to accumulate at high doses in the colonic tissue [30]. Lately, there is growing interest in designing clinical trials to test the potential beneficial effect of ASA/MET combinations to modulate the metastatic spread following the surgical resection of the primary mass [23,31].

In light of the CRC molecular heterogeneity, the design of effective personalized treatments would require a proper patient stratification [32], molecular profiling [33], and multidrug screening tests. The CRC heterogeneity regards both the primary tumor as well as locoregional lymph nodes, whose examination upon surgical resection is extremely important for prognosis and treatment [34,35]. Interestingly, biomimetic three-dimensional (3D) cultures of patient-derived cells tend to resemble the native tumor niche and preserve the original genotype and phenotype of malignancy [36]. In this work, patient-derived cancer cells, both from primary tumors and locoregional metastatic lymph nodes, were cultured in suspension as spheroids. Different 3D biological assays were performed to investigate the effect of ASA and/or MET on cancer cell viability, intratissue migration, and vascular adhesion to endothelial cells under flow. Extensive immunochemistry analyses were conducted to characterize the original cancerous phenotype and verify that the *in vitro* cultures maintained the molecular features of the tumor source.

Materials and Methods

Patient-Derived CRC Cell Isolation

CRCs with or without locoregional lymph node metastases were investigated. A total of 11 patients (8 males and 3 females, age between 55 and 93 years old, all Caucasian) with well-differentiated colorectal adenocarcinomas (stage I-IIIC) were selected for the present study. The patient could also carry diabetes with or without MET therapy prior to surgical resection. Patients undergoing chemotherapies, radiotherapy, and targeted therapies prior surgery were excluded from the study. Upon resection, colon carcinoma specimens were washed thoroughly in PBS and transferred into cold advanced DMEM/F12 (Invitrogen, 12634028) supplemented with 200 mM glutamine and a cocktail of antibiotics and antimicotics (100 U/ml streptomycin, 100 μg/ml penicillin, 2.5 μg/ml amphotericin, 0.01 mg/ml kanamycin, 50 μg/ml gentamicin, 5 μg/ml nystein). Specimens were minced in sterile conditions on ice, the suspension was then let to sediment, supernatant was discarded, and the tumor pieces were digested by Collagenase IV (Gibco, 17104-019, 7.14 mg in 10-ml medium) and DNaseI (Roche, cod. 11284932,001, 0.3-0.5 mg/ml). Ten milliliters of enzymatic solution is sufficient to digest about 0.7-1.5 g tissue. Digestion was performed at 37°C for 45 minutes. The digested tumor pieces were then passed through a 70-μm cell strainer, and the undigested pieces were digested for further 45 minutes. The digestion/filtration steps were performed in total two or three times until complete digestion is reached. Afterward, the flow through was filtered through a 40-μm cell strainer. The filtrate was centrifuged for 10 minutes at 180 ×*g*, and then the pellet was resuspended in stem cell medium containing the advanced DMEM/F12 supplemented with nutrients and growth factors [1× B27 minus vitamin A (Invitrogen, 12587010), 1× insulin-transferrin-selenium ITS-G (Invitrogen, 41400045), 4 μg/ml heparin (Sigma-Aldrich, H3149), 600 μg/ml glucose (Sigma-Aldrich, G7021), 9.7 μg/ml putrescine (Sigma-Aldrich, P5780), 20 nM progesterone (Sigma-Aldrich, P8783), 10 ng/ml bFGF (Peprotech, AF-100-18B), 20 ng/ml EGF (Peprotech, AF-100-15), 20 ng/ml HGF (Invitrogen, PHG0254)]. After counting, the isolated cells were seeded at the cell density of 2000 cells/well in nonadhesive GravityTRAPTM ULA 96× well plates (Insphero, ISP-09-001). Plates were centrifuged 2 minutes at 250 ×*g* to allow cell deposition at the bottom of the wells where they could start self-aggregate. Cells were cultured at 37°C in a 5% CO_2 humidified incubator. Half of the medium was replaced with fresh medium every other day. Spheroid formation occurred between 3 and 6 days after seeding. Once generated, spheroids could be embedded in a collagen matrix.

Cell Lines

Human umbilical vein endothelial cells (HUVEC) were obtained from PromoCell and were cultured using Endothelial Cell Growth supplement-mix Medium (PromoCell) supplemented with 10% FBS (GIBCO). Cells were used until passage 7. HCT-15 cell line (American Type Culture Collection) was selected due to the high-invasiveness character. Cells were cultured in standard RPMI-1640 medium supplemented with 10% FBS, 100 U/ml streptomycin, 100 μg/mL penicillin, and 200 mM l-glutamine. Medium was renewed every second day, and cells were used at passage 8-10 in all experiments. To generate spheroids, 500 cells in 80 μl were seeded as described in the "patient derived CRC cell isolation" section. Spheroids were kept in culture for 24 hours prior to encapsulation into the collagen.

Spheroid Embedding Into a Collagen Matrix

Collagen from bovine skin was used (Sigma-Aldrich, C42C43). Gels were prepared by quickly premixing the collagen solution with a buffer solution (1 N NaOH, HEPES, pH 7.4) to achieve a collagen final concentration of 1.5 mg/ml (pH 7-7.4). The spheroid was embedded in the mix and loaded into either 24× well plates or 8× Nunc Lab-Tek chamber slides (Sigma-Aldrich, C7182). The hydrogel was let to polymerize at 37°C for 1 hour, and then culture medium was added. ASA (Sigma-Aldrich, A2093) and MET (Sigma-Aldrich, PHR1084) were added, either alone or combined, to the culture medium at 1, 5, and 10 mM each for up to 7 days. Medium was changed every second day.

Migration Assay

Spheroids embedded in collagen were imaged at day 1, 4, and 7 via optical microscopy (Leica 6000 inverted microscope). Images were processed with ImageJ, and data were collected using Excel. Statistical analyses were performed with OriginPro8 applying two-way analysis of variance test with Bonferroni's post hoc test ($\alpha = 0.05$).

Immunofluorescence

Immunofluorescence was carried out as described before on 3D cell cultures [37]. Primary antibodies were: anti-active β-catenin (anti-ABC) clone (8E7 05-665 EMD-Millipore Corp., USA) (1:300), CD323/EpCAM Ms anti-HU mAb clone VU-1D9, FITC conjugate (Molecular Probes Life Technologies REF A15755) (1:100), Keratin 20 (D9Z1Z) XP (R) rabbit mAb (13063S Cell Signaling Technology) (1:400), CD133 (D2V8Q) (XP) (R) Rabbit mAb (64326S Cell Signaling Technology) (1:400), CDX2 (D11D10) Rabbit mAb (12306S Cell Signaling Technology) (1:50), and Ki-67 (85D) Mouse mAb (944T Cell Signaling Technology) (1:800). Secondary antibodies, all from Invitrogen (1:500), were: Alexa Fluor 488 goat anti-mouse IgG (A11029), Alexa Fluor 647 goat anti-rabbit (A21245), Alexa Fluor 568 goat anti-rabbit (A11036), Alexa Fluor 568 goat anti-mouse (A11031), and Alexa Fluor 647 goat anti-mouse IgG (A21236). Hoechst was used to label the nuclei. Images were acquired using the confocal Nikon A1 microscope and then were processed with Image J.

Histological Evaluation

CRC specimens were fixed in formalin and embedded in paraffin wax. Paraffin sections of 5-μm thickness were stained with hematoxylin/eosin for microscopic evaluation to establish the diagnosis of CRC according to the WHO Digestive System Tumors and to evaluate malignancy. Further, fixed CRC sections were treated with anti-CK20 (clone SP33, Ventana) and anti-CDX2 (clone EPR2764Y, Cell Marque) antibodies to confirm the colon origin of the lesions via immunohistochemistry. Immunohistochemistry

was performed using an automated instrument (BenchMark ULTRA, Ventana).

Viability Assay

The Apoptosis/Necrosis Detection Kit (blue, green, red) (ABCAM, Ab176749) was used according to the manufacturer's protocol. This kit allows to distinguish between viable cells, apoptotic cells, and necrotic cells via fluorescence microscopy. Images were acquired using the confocal Nikon A1 microscope and then were processed with Image J. Statistical analyses were performed with OriginPro8 applying two-way analysis of variance test with Bonferroni's post hoc test ($\alpha = 0.05$).

Scanning Electron Microscopy (SEM)

SEM analysis was performed to evaluate the morphology of spheroids developed from HTC-15 cell line and from patient-derived primary tumor cells. Samples were fixed for 2 hours in 2% glutaraldehyde in 0.1 M cacodylate buffer. After fixation, they were washed three times with the same buffer and post-fixed for 1 hour in 1% osmium tetroxide in distilled water. After several washes with distilled water, the samples were dehydrated in a graded ethanol series, 1:1 ethanol:hexamethyldisilazane, and 100% hexamethyldisilazane and dried overnight in air. Dried samples were then mounted on stubs using silver conductive paint and coated with gold. SEM images were collected with a scanning electron microscope (Elios Nanolab 650, FEI) at accelerating voltage of 5-15 keV.

Microfluidic Chip Fabrication

The single-channel microfluidic chip was fabricated as described before [38]. Briefly, an SU8-50 master was used as a mold for PDMS replicas of the chip. First, a 40-μm-thick layer of SU8-50 photoresist (MicroChem) was spin coated on a silicon wafer. Then, the negative SU8-50 template was pre- and soft baked for solvent evaporation, exposed to UV light and baked again for epoxy crosslinking, and finally developed. This template was replicated using a mixture of PDMS and curing agent Sylgard 182 (Dow Corning Corporation). After peeling off the template, the channel extremities of the PDMS replica were punched via a biopsy puncher (OD, 1 mm, Miltex) to form inlet and outlet ports. Finally, PDMS replica was sealed with a glass slide ($20 \times 60 \times 0.17$ mm) (No. 1.5H, Deckalgaser) via oxygen plasma treatment. The resulting microfluidic chip had a rectangular cross section with 210-μm width, 42-μm height, and 2.7-cm port-to-port length.

Seeding of Endothelial Cells Into the Microfluidic Chip

Sterilized chips were covered with 20 μg/ml fibronectin to allow cell adhesion. HUVECs were introduced in the channel from the inlet port at a density of 10^6 cells/ml by using a pipette tip. Then, chips were placed in an incubator to allow cell attachment and growth and continuously perfused with culture medium until cell confluence. HUVEC monolayers were inflamed, at the occurrence, with 25 ng/ml of TNF-α for 12 hours. After inflammation, the endothelium was treated with ASA and/or MET (1 mM in total) for 5 hours followed by the cancer cell rolling experiment.

Cancer Cell Adhesion and Rolling Under Dynamic Conditions

The microfluidic chip was placed on the stage of an epifluorescence inverted microscope (Leica 6000). The working fluid was injected into the chip using a syringe pump 33 Dual (Harvard Apparatus). After dissociation of the spheroid, CRC cells (or HCT-15 cell line) were incubated for 30 minutes with CM-Dil at 37°C (0.5%, Thermofisher) according to the manufacturer's protocol. Then, the cells were washed thoroughly in PBS to remove the excess dye. Finally, cells were resuspended in medium at the density of 10^6 cells/ml and were introduced via a syringe pump on the HUVEC monolayer inside the microchannel. Following cell rolling, a washing step with PBS was performed to remove the non adherent cancer cells from the endothelium. The inlet of the chip was connected to the syringe pump through a polyethylene tube (BTPE-60, Instech Laboratories), while the tube of the outlet port was in PBS, to ensure flow equilibrium. After 1 minute flow, the interaction of cancer cells with HUVECs was recorded for 15 consecutive minutes for each experiment. The flow rate imposed via the syringe pump was 100 nl/min.

Cytotoxicity Assay for Endothelial Cells

A total of 10^4 HUVECs or HCT-15 were plated in 96-well plates and after 24 hours were incubated with ASA and/or MET (1 mM in total) for 24, 48, and 72 hours. MTT (Sigma-Aldrich, 5 mg/ml) was added to the medium for 3 hours. Next, each well was emptied out and 1 ml 100% ethanol was added. Absorbance at 570 nm was measured via a spectrophotometer (mQuanti). Values of absorbance were expressed as percentage of MET/ASA cytotoxicity.

Immunostaining and Confocal Microscopy Analysis of the Microchips

After cancer cell rolling over the endothelium, the chips were fixed with 3.6% paraformaldehyde (Sigma-Aldrich) for 15 minutes at RT. The channel was washed three times with PBS, and cells were permeabilized with 0.1% Triton X-100 for 10 minutes on ice followed by three washes with PBS. Then, they were incubated with 20% goat serum (Sigma-Aldrich) for 30 minutes and then incubated for 3 hours with mAb mouse Ve-cadherin (Abcam, 1:100) in 10% goat serum at 4°C. After several washes with PBS, cells were incubated 50 minutes with the mAb goat FITC conjugated (Abcam, 1:500) and Hoechst. After washing, chips were imaged with the Nikon A1R-A1 confocal microscope.

Results

Primary Cancer Cell Isolation and CRC Spheroid Formation

This is a translational study conducted between 2018 and 2019 on eleven patients operated for CRC at Galliera Hospital. The study was approved by the Regional Ethical Committee (code 6UCS2016; July 16, 2016). Demographic, clinical, pathologic, and follow-up data were obtained from patients' medical records. All the patients treated with chemotherapy, radiotherapy, or targeted therapy were excluded from the study. A protocol for the isolation of CRC cells from surgical specimens was established. The protocol was initially developed and optimized using murine samples and then applied to tissues derived from CRC patients. The main steps of the procedure are schematically shown in Figure 1*A*. A typical patient sample ranged from a few hundreds of milligrams to about 1 g. The tissue was mechanically dissociated to obtain small pieces of about 1 mm in diameter. Then, these pieces were further dissociated enzymatically with collagenase IV. Following isolation, cells were seeded into a microgravity 96-well plate, which promoted cell aggregation over adhesion to the substrate. After 3 to 5 days, cells formed a well-defined spheroid in suspension (Figure 1*B*). From the original human specimen, a few millions of cells and hundreds of ~100-μm tumor spheroids were routinely generated.

Analysis of Cell Migration on Patient-Derived CRC Spheroids

In order to assess the metastatic potential of patient-derived CRC cells, a 3D migration assay in a collagen matrix was realized. Out of the eleven patients included in the study, three patients did not give a sufficient number of spheroids and were eliminated from the present study. Therefore, the experiments of 3D migration were performed on eight patients. Figure 2*A* shows a schematic representation of a spheroid in a collagen matrix where two main regions can be identified: “tumor core” (white dashed line in the center) with densely packed tumor cells; “migration region” (blue dashed line) with elongated and more spread tumor cells. Representative bright field images are shown in Figure 2*B*, where spheroids with their

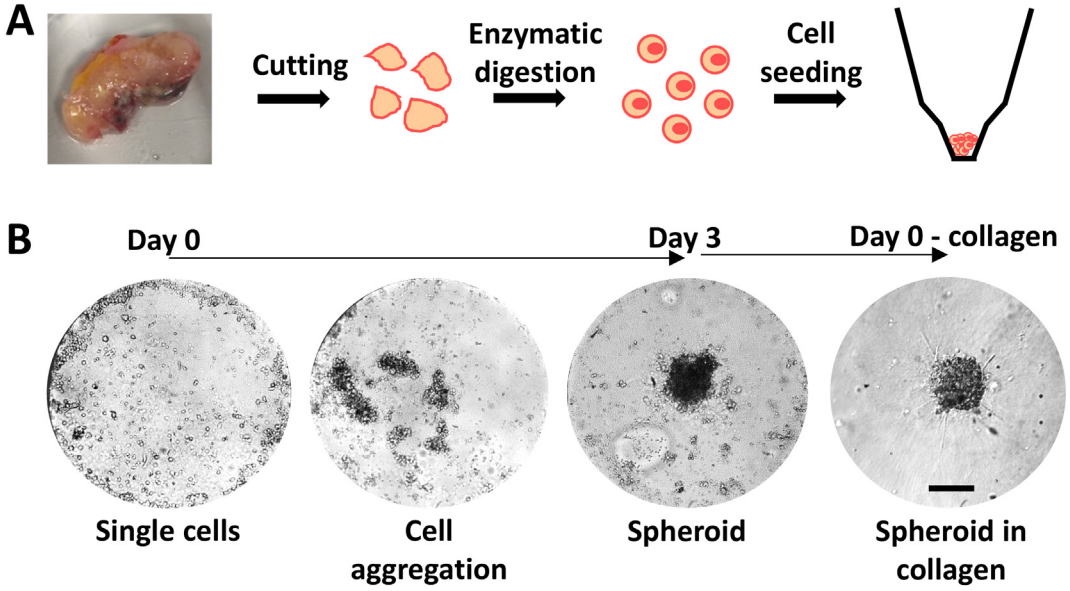

Figure 1. Formation of spheroids from patient derived colorectal cancer specimen. (A) Schematic representation of the procedure for cancer cell isolation from human-derived specimen, including cutting, enzymatic digestion, and cell seeding into microgravity conic well plates. (B) Representative bright-field images of spheroid formation from single cell suspension in a time window of 3 days and spheroid embedding in 3D collagen matrix (scale bar 100 μm).

core and migration areas are clearly highlighted at different time points, namely, day 1, 4, and 7, post spheroid embedding into the collagen matrix. The size of these two regions was quantified (Figure 2C). While the tumor core size did not change significantly, the migration region increased over time for all considered samples. The migration region doubled in diameter from day 1 (~100 μm) to day 4 (~200 μm) and increased up to ~250 μm at day 7. This clearly documents the spreading propensity of these patient-derived CRC cells.

To assess the potential of ASA and MET in blocking tumor metastasis, CRC spheroids in 3D collagen were treated with three different concentrations (1, 5, and 10 mM) of ASA and MET, either alone or in combination. The conventional IC50 values for ASA and MET on CRC cell line (HCT-15) monolayers are in the order of several millimolars (Supplementary Figure S1). The size of the tumor core and migration area was determined via optical microscopy over time up to 7 days, as shown in Figure 3, *A* and *B*, respectively. As per the tumor core, after 7 days of culture, a moderate statistically not significant reduction in size was observed for the control untreated spheroids. This is probably due to the high variability among different patients in terms of gene expression and mutation profiles, as reported in the literature [39]. Similarly, no statistically significant changes were observed in tumor core size for the ASA and MET treatment groups. However, at day 7, the ASA- and MET-treated spheroids appeared dark

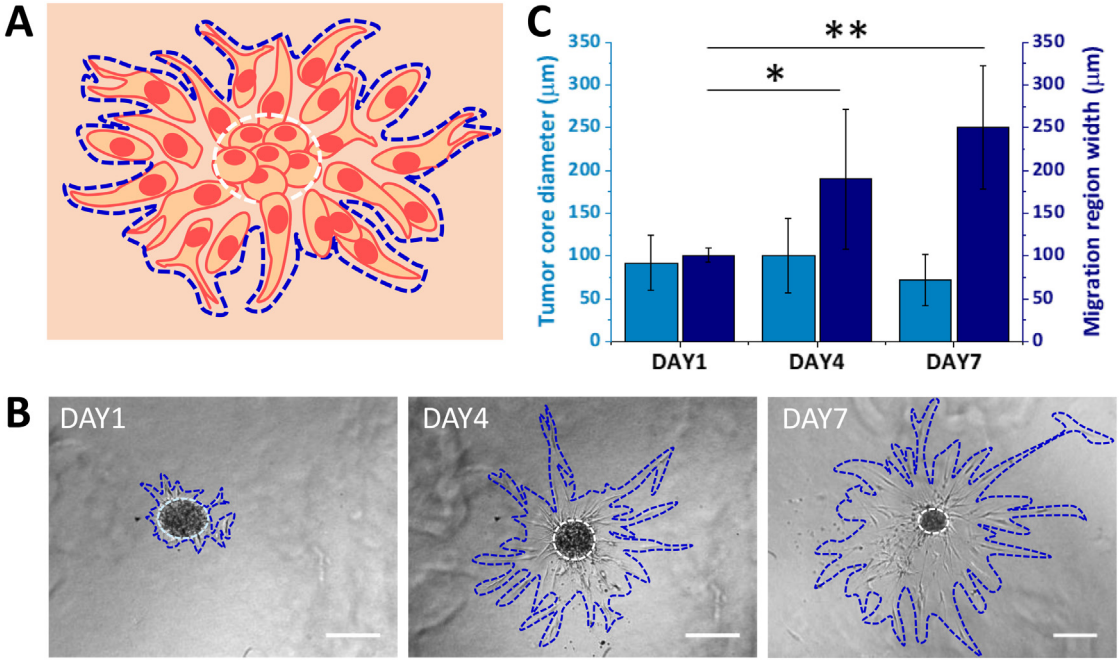

Figure 2. Analysis of CRC spheroid growth and cell migration in a 3D collagen matrix. (A) Schematic representation of a cancer cell spreading from the original spheroid into the collagen; dash lines indicate the tumor core (white) and the migration region (blue). (B) Representative bright-field images of the same spheroid obtained from patient 1 over time (scale bar 200 μm). (C) Quantification of tumor core size and cell migration over time ($n = 8$ patients) ($^{*}P < 0.05$, $^{**}P < 0.005$).

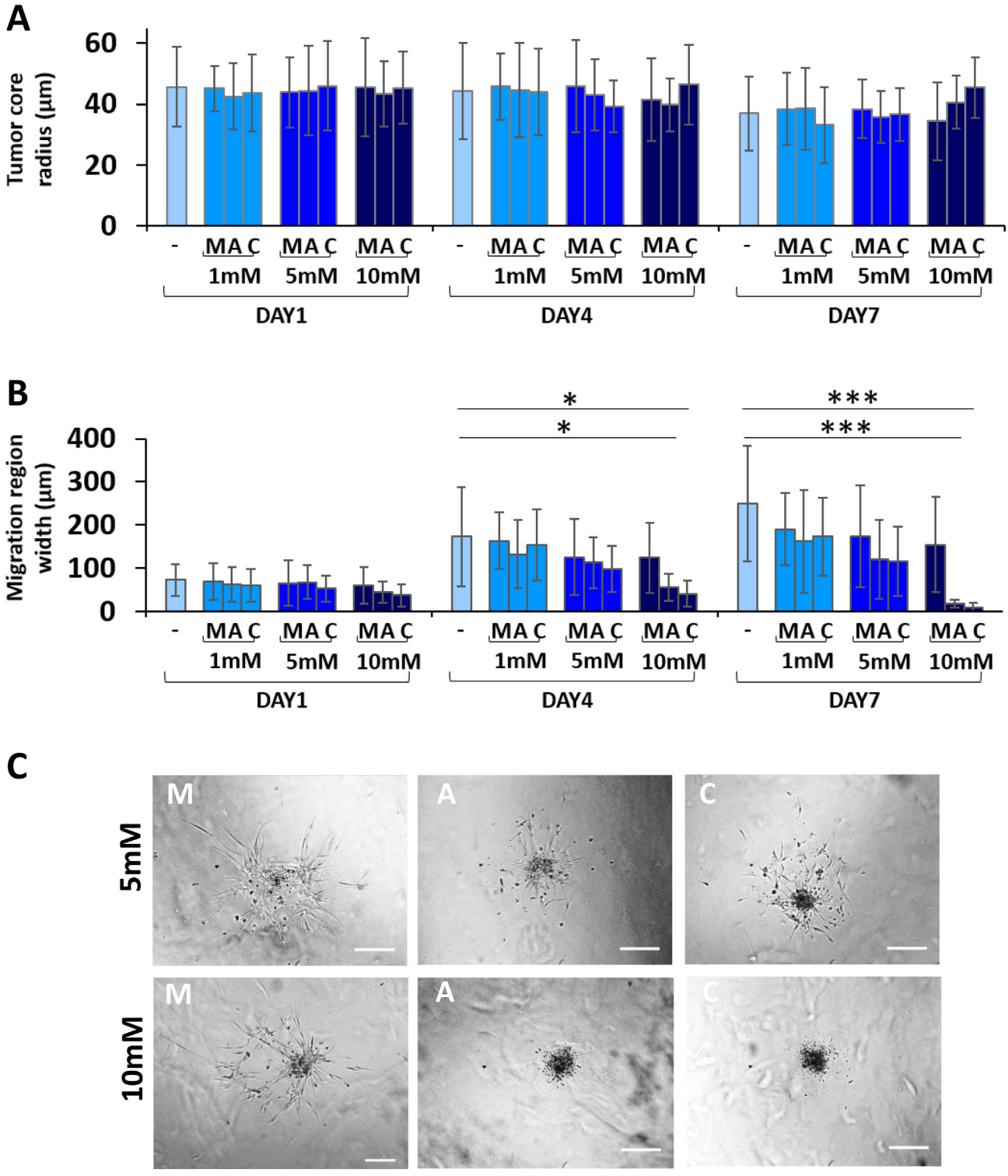

Figure 3. Analysis of CRC spheroid response to ASA and MET treatment. (A) Quantification of CRC spheroid core size in a cohort of eight patients. (B) Quantification of 3D migration region for CRC spheroids ($n = 8$) (*$P < 0.05$; ***$P < 0.0005$). (C) Representative bright-field images of spheroids from one patient at day 7 (scale bar 200 µm) (− = control; M = MET; A = ASA; C = ASA/MET combination).

and shrunk as compared with the control groups, which is a first sign of cell death and sufferance. More interestingly, Figure 3*B* details the variation of migration area over time. This was significantly diminished by the exposure to ASA and the ASA/MET combination. This effect was already observed at day 4 but became more evident at day 7. The effect of ASA on impairing migration was clear already but not significant at drug concentrations of 5 mM (Figure 3*B-C*). This can be again ascribed to the high variability in invasive potential and CRC stage among patients, which caused a high standard deviation among the experimental replicates. However, at the highest doses of 10 mM, the decrease in the migration area became significant as compared to the control. Migration was reduced by ~60% in the ASA group and ~50% in the ASA/MET-treated samples at day 4; migration was further decreased by over 90% for both treatments at day 7. Interestingly, the same analysis was also performed on the HCT-15, a well-known

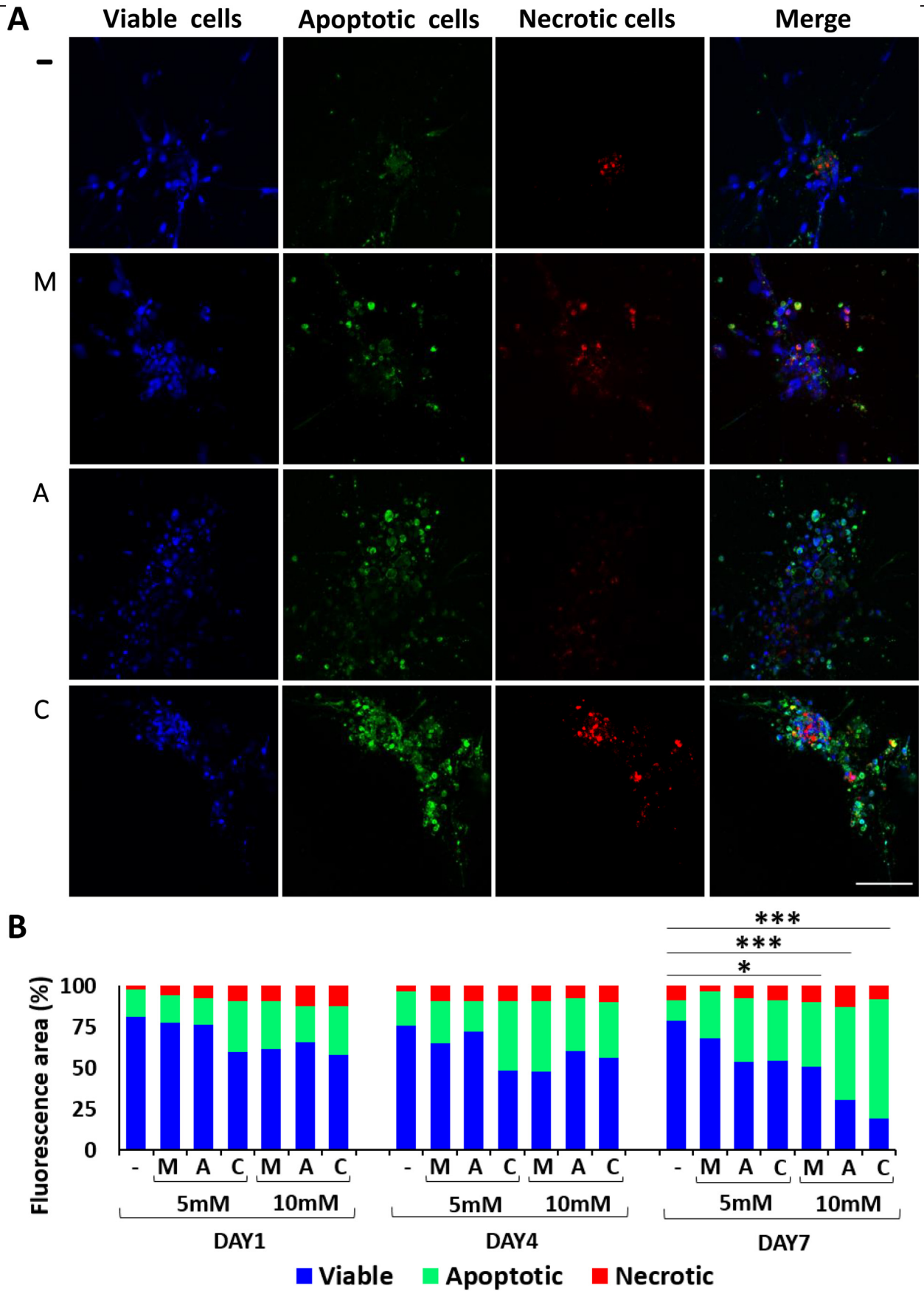

(caption on next page)

colorectal cancer cell line, where a similar trend was observed (Supplementary Figure S2). Nevertheless, the reduction in migration area was not statistically significant for the HCT-15. Once more, this difference in therapeutic response highlights the limitations of clonal cell lines over human primary cells.

Analysis of Cell Viability in Patient-Derived CRC Spheroids

The cytotoxic effect of the two drugs and their combination on the tumor spheroids was explored. Since at low doses (1 mM) no effect was observed either on migration or tumor core size, this treatment condition was not considered in the following viability assay. Briefly, tumor spheroids were embedded into a collagen matrix and treated with ASA and MET, either alone or combined, and then viability was tested at the same time points used in the migration studies. A colorimetric kit was used based on three fluorescent dyes, namely, calcein for cell viability (blue), apopxin for cell apoptosis (green), and 7-AAD for necrosis (red). Figure 4*A* shows representative confocal images of the spheroids at day 7 upon treatment with ASA 10 mM (A), MET 10 mM (M), or a combination (C) of the two drugs at 10 mM each. The first row in Figure 4*A* is related to the untreated spheroids (−). The bar chart of Figure 4*B* shows the temporal variation of three different cell conditions (viable, apoptotic, necrotic) over the entire cell population. At day 1 and 4, for all conditions, most cells were observed to be viable (blue bar), a modest number (considerably lower than 50%) of cells were apoptotic (green bar), and an even smaller number of cells, which mainly localized at the spheroid core, were necrotic (red bar). The percentage of necrotic cells remained constantly low (~9%) over time and was not affected by the treatments. This would imply that necrosis should mostly be ascribed to low oxygen concentration in the core of the tumor spheroid rather than an actual pharmacological effect exerted by ASA and MET. Instead, the number of viable and apoptotic cells at high doses, at day 7, was reversed as compared to the untreated control. In particular, the control was characterized by 78% viable cells, while the treatments with the drugs at 10 mM caused extensive apoptosis, obtaining 39% apoptotic cells with MET, 56% with ASA, and 72% with the ASA/MET combination, all values being statistically significant compared to the percentage of apoptosis (12%) in the control conditions ($P = .04$ for control versus MET; $P = 4.74 \times 10^{-6}$ for control versus ASA; $P = 5.18 \times 10^{-10}$ for control versus ASA/MET). These data indicate that the reduction in cell migration observed in Figure 3 has to be ascribed at least partly to cell death. It is worth noting that the ASA/MET combination determined a further increase in the apoptotic effect compared to the single treatments, suggesting that the two drugs may have an additive or even synergistic effect, as recently suggested [40].

Recalling the MTT assay conducted on HCT-15 cells and documented in the Supplementary Figure S1, it is observed that ASA and the ASA/MET combination inhibited HCT-15 cell growth at concentrations > 5 mM (IC50 = 6.30 mM). On the other hand, MET showed a minor cytotoxicity. This appears to be in line with the data deduced for the CRC spheroids where again ASA and ASA/MET were more effective in containing cell migration (Figure 3*B*).

Analysis of Biomarkers in Patient-Derived CRC Spheroids

It is important to highlight here that, during the human specimen processing (Figure 1), cells were not sorted based on their tumor markers. Thus, in contrast with spheroids from HCT-15 cells, the patient-derived spheroids should include a heterogeneous population of cells resembling the typical multicellular nature of the native tumor niche [41]. This heterogeneous nature was also captured by the scanning electron micrographs in Supplementary Figure S3, where the surface of CRC primary spheroids appears more irregular as if composed by cells of different size and type, in contrast with the smoother and more homogeneous surface of HCT-15 spheroids. In order to verify the presence of colon cancer specific cells in the spheroids, immunostaining and confocal imaging were performed. In particular, the colorectal cancer biomarkers CDX2 and CK20 were tested in collagen-embedded spheroids. CDX2 is a nuclear transcription factor, whereas CK20 is a cytokeratin of the intermediate filaments of cytoskeleton. These markers were tested at 4 days after spheroid embedding into collagen, when already a cell migratory behavior could be observed. As CDX2 and CK20 are routinely used for the immunohistochemistry of surgical specimen, their presence was positive in the histological sections from the patients under this study (Supplementary Figure S4). Accordingly, CRC spheroids stained positively for CDX2 and CK20 (Figure 5*A*), confirming that they did include colorectal cancer cells.

The heterogeneity in cell phenotypes and the prevailing cancerous origin of most of the cells were further confirmed using antibodies specific for CD133 and ESA, which are cancer stem cell markers typically found in carcinomas. Indeed, while migratory cells expressed the colon cancer biomarker β-catenin, a subpopulation of the tumor spheroids, mainly located at the core, consisted of $CD133^+$ and ESA^+ cancer stem cells (Figure 5*B*). Notice that these cells are generally considered responsible for the proliferation and invasive potential of tumors. Also, it should be here recalled that cancer stem cells are considered the most resistant to chemotherapeutics, mostly due to their quiescent nature [42].

Finally, as MET and ASA are normally targeting cell metabolic pathways [20], the effect of MET and ASA on the proliferation marker Ki-67 was evaluated. As shown in Figure 5*C*, a short-term treatment of 4 hours did not affect the marker expression. However, treatments at 10 mM caused a visible reduction of proliferation as compared to the control at 7 days.

Analysis of Vascular Rolling and Adhesion for Isolated Patient-Derived CRC Cells

Primary CRC cells were also used as single cells to investigate their rolling and adhesion potential in a microfluidic chip (Figure 6*A*) [38, 43–45]. A continuous layer of endothelial cells (HUVEC) was developed within the chip, mimicking the vascular walls (Figure 6*B*). Inside the microfluidic chip, a solution of suspended cells can be injected via a syringe pump and imaged while rolling on the endothelium using a fluorescence microscope. The microfluidic chip of Figure 6, *A-B* comprises a single channel with a 210-μm width and 42-μm height. A cell suspension was infused at 100 nl/min. To promote local adhesion, HUVECs were pretreated with TNF-α (25 ng/ml overnight). As shown in Figure 6, *C-D*, the number of cells adhering to the endothelium increased with the TNF-α conditioning. Nevertheless, when the endothelium was treated with MET, ASA, or the combination (1 mM total), the adhesive properties of the endothelium were altered, thus causing a reduction in the vascular deposition of cancer cells. In particular, MET caused a 31% reduction, ASA induced a 49% reduction, and the combination of the two drugs led to a 61% reduction. The same vascular adhesion experiment was also conducted with the HCT-15 cells (Supplementary Figure S5, *A-B*). The same trend as for the primary cells was confirmed with the combination of ASA and MET inducing the most significant decrease in vascular deposition. This continues to support the initial observation on the therapeutic effectiveness of the combination. Notice, once more, that the inhibition of cell adhesion was more evident for the primary cancer cells rather than the HCT-15 cells. As in these adhesion experiments, the intervention was directed against the endothelium, the cytotoxic effect of MET and ASA on HUVECs was assessed using an MTT assay. This control experiment (Supplementary Figure S5*C*) confirmed that MET and ASA did not exert any cytotoxic effect on HUVECs

← **Figure 4.** Effect of MET and ASA on cell apoptosis/necrosis in CRC spheroids embedded in a 3D collagen matrix. (A) Representative confocal images (maximum intensity projection of *z*-stacks) of control and treated spheroids at 10 mM at day 7 (green cells: apoptotic; red cells: necrotic; blue cells: viable) (−: control; M: MET; A: ASA; C: ASA/MET). (B) Chart quantifying the relative abundance of viable, apoptotic, and necrotic cells within the patient-derived CRC spheroids. Quantification bar chart (n = 3 patients) (*$P < .05$, ***$P < .0005$) (− = control; M = MET; A = ASA; C = ASA/MET combination).

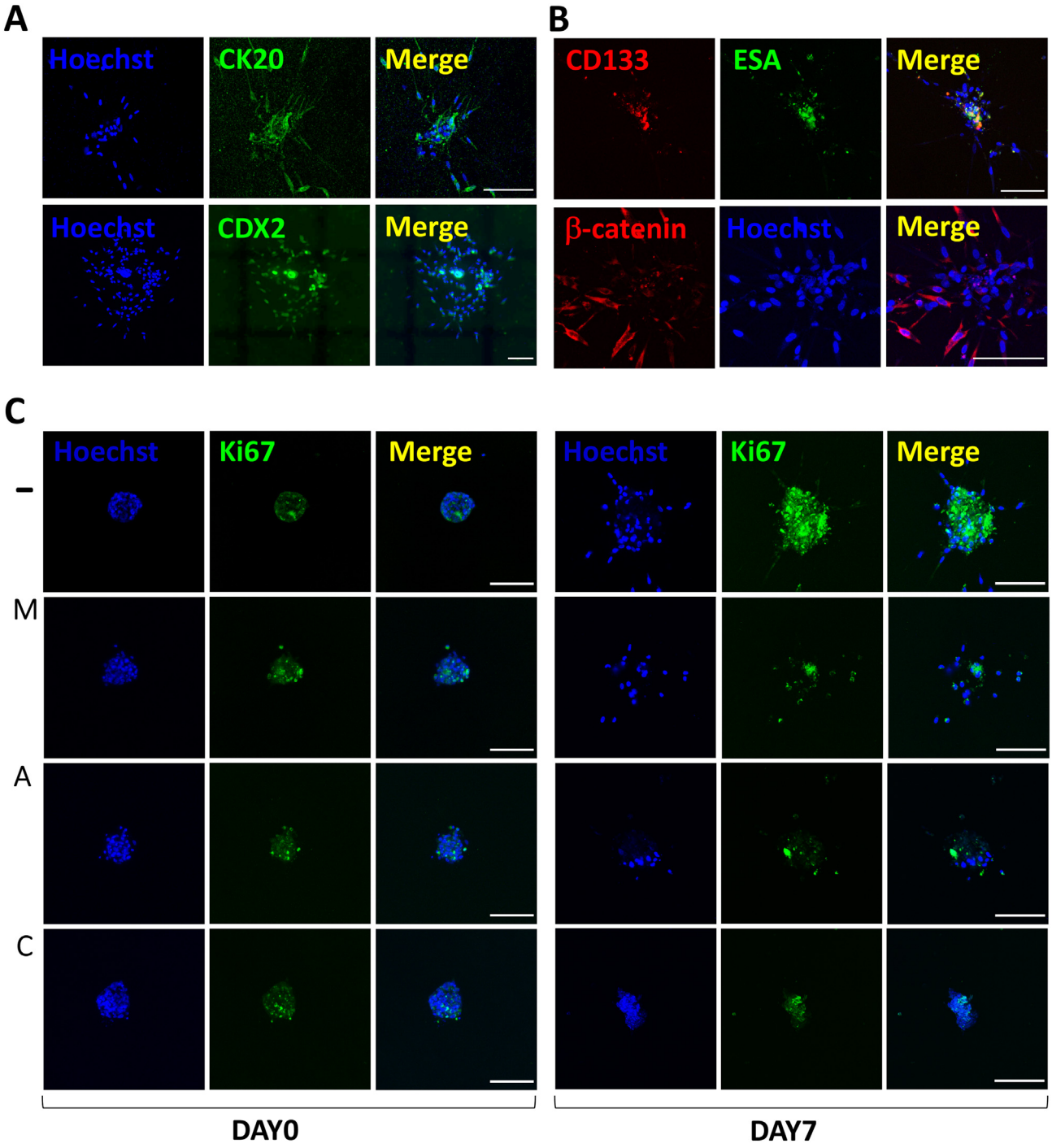

Figure 5. Immunofluorescence of biomarkers in patient-derived CRC spheroids. Representative confocal images (maximum intensity projections of *z*-stacks) of cancer spheroids stained at day 4 post spheroid embedding in collagen for the (A) CRC biomarkers CK20 and CDX2; (B) cancer stem cell biomarkers ESA and CD133 at day 4; (C) active form of β-catenin, i.e., a molecular marker known to be active in CRC. (D) Representative confocal images of the proliferation marker Ki-67 at day 0 and day 7 (scale bar 100 μm) (– = control; M = MET; A = ASA; C = ASA/MET combination).

at the concentrations used to inhibit cancer cell adhesion (1 mM). Notice that the migration assay with the 3D tumor spheroids and the microfluidic chip analysis would suggest that the two drugs were able to mitigate cancer cell spreading by acting on the vascular and extravascular migration.

Tumor Spheroids from Patients Sensitive to MET

For five out of eight patients with successful generation of *in vitro* spheroids, these did not respond to MET treatment in the migration assay even at the highest dose (i.e., 10 mM). However, for three patients, MET showed to significantly affect the size of the migration area, reducing it to 25% as compared to control ($P = .028$) (Figure 7*A-B*). One of the latter two patients gave rise to small spheroids with low viability and low migration capacity, and this can explain the high standard deviation in the control group. By examining the clinical history of these patients, it resulted that one was diabetic, while the other two were neither diabetic nor insulin resistant.

As mentioned previously, the protocol of cell isolation and spheroid formation was not successful for three patients out of eleven patients under study. The clinical history of these three patients showed common features: they were all diabetic and were daily pretreated with the antidiabetic drug

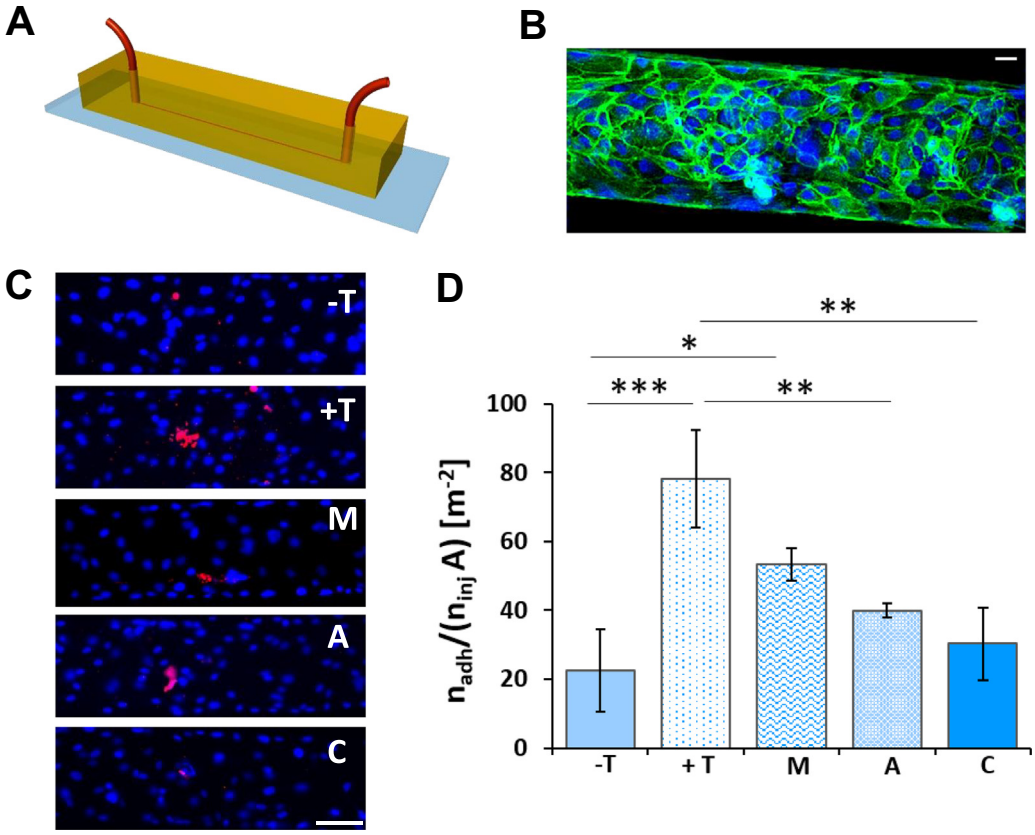

Figure 6. CRC cell adhesion on the endothelium into a microfluidic chip. (A) Schematic of the microfluidic channel (length = 2.7 cm, width = 210 μm, height = 42 μm). (B) Representative confocal 3D image of a confluent layer of HUVEC cells covering the inner walls of a microfluidic channel. Cell nuclei are stained in blue with Hoechst; Ve-cadherin is stained in green (scale bar 50 μm). (C) Representative fluorescent images of adhering cells on HUVEC monolayer, (− T = control; + T = with TNF-α 25 ng/ml; M = MET 1 mM; A = ASA 1 mM; C = ASA/MET combination 1 mM) (scale bar 200 μm). (D) Quantification of adhering cells on endothelium, Q = 100 nl/min (n = 3 patients) (*P < .05; **P < .005; ***P < .0005).

MET. These findings would further support the hypothesis that when MET is regularly administered to a diabetic patient, it can decrease the aggressiveness and invasiveness of colorectal cancer cells to the point that not even spheroids can be generated out of their clinical samples. Only one of the three specimens from these diabetic patients gave rise to a modest spheroid formation, corresponding only to about 20% of the total number of wells initially seeded with cells. This quantity was indeed not enough for carrying out systematic migration and viability assays. Nonetheless, the few collected spheroidal-like structures were embedded in collagen to follow the proliferation marker Ki-67 via immunostaining over time. As shown in Figure 7*C*, tumor spheroids from a diabetic patient pretreated with MET showed almost no staining for Ki-67 at day 0. This would indicate that the newly formed spheroids did not include proliferating cells. On the contrary, after 7 days in culture, cells started migrating and expressing Ki-67. This evidence may suggest that whenever cancer cells find a supportive environment, they start again to proliferate. Possibly, these observations highlight the importance of a continuous and sustained treatment with MET in diabetic patients affected by CRC.

Tumor Spheroids from Metastatic Lymph Nodes

Not surprisingly, three of the eight patients with successful generation of *in vitro* spheroids showed also metastasis in the locoregional lymph nodes. Using the same protocol of tissue digestion and cell isolation described in Figure 1, colorectal cancer cells from metastatic lymph nodes were successfully isolated. These lymph node–derived spheroids exhibited a behavior similar to that of the spheroids originated from the primary tumor (Figure 8, *A-B*). In particular, after 7 days of treatment, ASA and MET at 10 mM reduced cell migration by 90% and 70% compared to the control, respectively. The migration was completely impaired when combining ASA and MET at 10 mM each. This continues to confirm the previous observation on the additive and synergistic effects of the ASA/MET combination. Focusing on the effect of MET, it is interesting here to notice that this drug did not show any effect for the primary tumor spheroids (n = 8), whereas a clear decrease in cell migration was induced in the lymph node–derived spheroids (n = 3). This was due to the fact that two of the three patients with locoregional lymph node metastasis were MET-sensitive patients not pretreated with MET (i.e., a diabetic patient and one non diabetic patient). Interestingly, the spheroids from these two patients were particularly sensitive to MET at the level of both primary tumor and metastatic lymph node, thus further supporting the use of this drug for mitigating cancer progression in MET-sensitive patients.

Discussion

The presented data show that patient-derived CRC cells can be routinely isolated from both primary malignant masses and metastatic lymph nodes. This is the first time, to authors' knowledge, that cancer cells were isolated from locoregional metastatic lymph nodes and employed, together with cells from the primary tumor mass, to develop a personalized screening for anti-metastatic drugs. The overall study confirmed that patient-derived cells are a more reliable system compared to cell lines, which are traditionally used in tumor biology and pharmacology studies. A 200-mg specimen of human malignant tissue was sufficient to generate a multitude of cancer cells to conduct different drug screening assays. The proposed protocol allowed us to boost tumor cell proliferation in suspension, establishing, in a short time, hundreds of tumor spheroids while preserving the original phenotype. Cancer spheroids have been recently demonstrated to

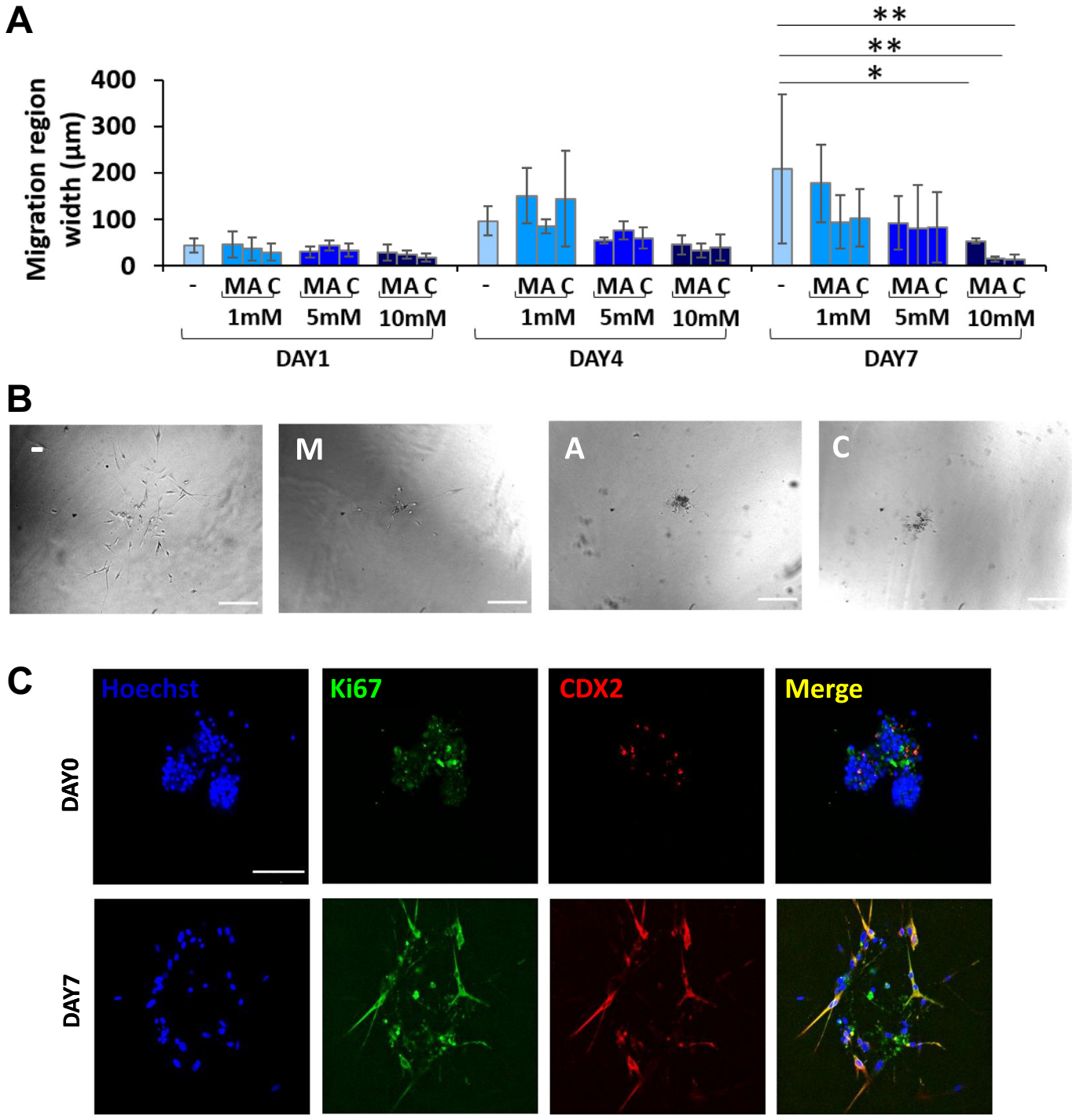

Figure 7. Analysis of CRC spheroids obtained from a subgroup of MET sensitive patients. (A) Quantification of 3D cell migration for MET-sensitive patients ($n = 3$ patients) (*$P < .05$; **$P < .005$) (− = control; M = MET; A = ASA; C = ASA/MET combination). (B) Representative images of CRC spheroids from a diabetic patient at day 7 (scale bar 200 µm). (C) Immunofluorescence images of CRC spheroids obtained from a patient affected also by diabetes pretreated with MET. Staining for the proliferation marker Ki-67 at day 0 and day 7 after spheroid embedding in 3D collagen (scale bar 100 µm).

be invaluable 3D tumor models not only *in vitro* but also in preclinical models as compared to the classic 2D cell cultures and *in vivo* injectable cell suspensions, respectively [46]. In line with this, the CRC spheroids generated in this study preserved the original heterogeneity of the native tumor niche [41], including the presence of migrating $CDX2^+$ and $CK20^+$ colorectal cancer cells and a central core of $CD133^+$ and ESA^+ cancer stem cells. The latter cells have been recognized to be resistant to chemotherapeutics, mostly because of their dormant state [42]. Furthermore, as *in vitro* models of tumors are used to predict drug efficacy [47,48], here multiple 3D *in vitro* screening assays were conducted using primary cancer cells. Specifically, cancer spheroids were embedded in a 3D collagen scaffold mimicking the extracellular matrix of CRC [49] to test 3D cell migration, cell viability, cell proliferation, and biomarker identification. In parallel, 3D microfluidic chips mimicking the microcirculation conditions [43] were adopted to investigate the vascular rolling and adhesion of cancer cells. Using these various assays, the two repurposed drugs, ASA and MET, were found to interfere with the distant dissemination of the malignant cells by tackling both tissue invasion and vascular transport. These

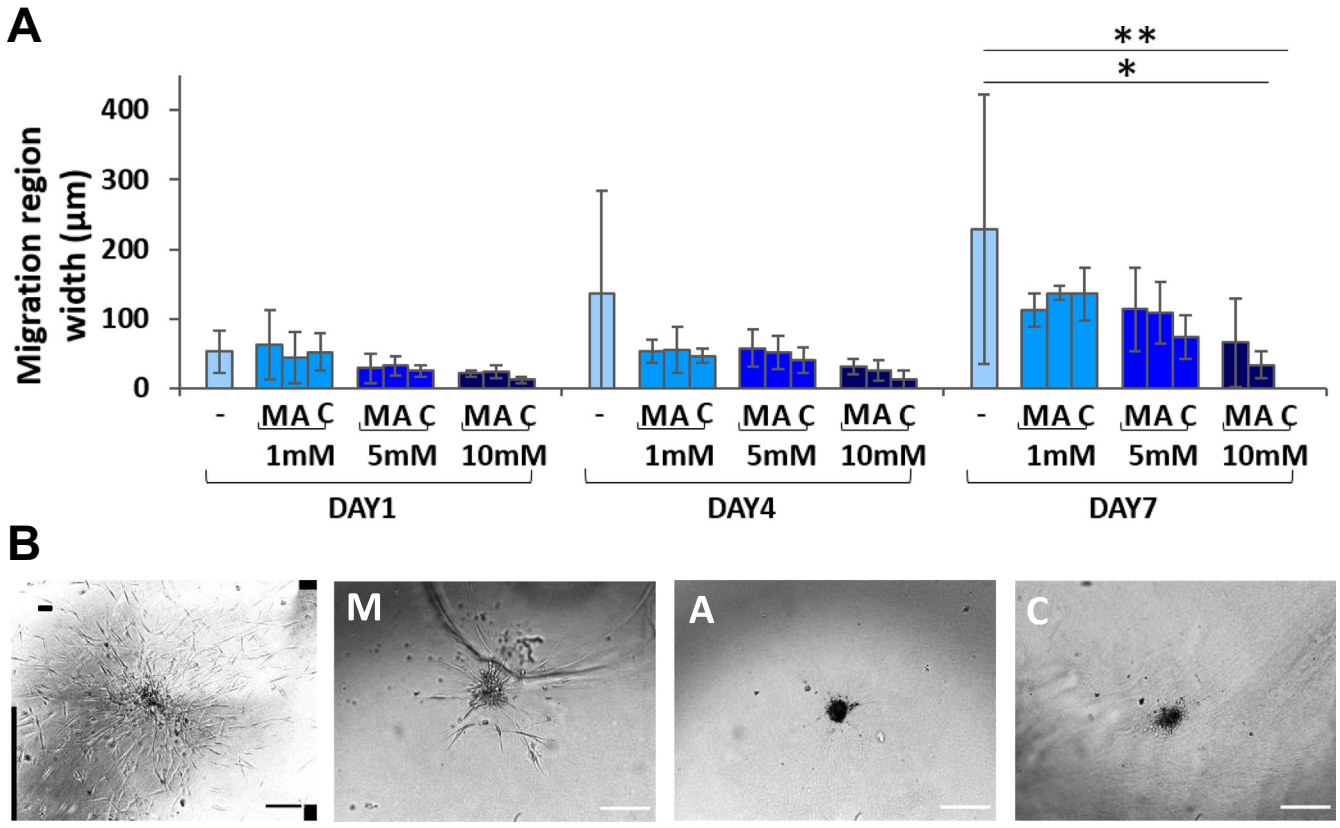

Figure 8. 3D migration of hCRC spheroids derived from metastatic lymph nodes. (A) Quantification of 3D cell migration ($n = 3$ patients) (*$P < .05$; **$P < .005$). (B) Representative bright-field images of hCRC spheroids from metastatic lymph node at day 7 (scale bar 200 µm) (− = control; M = MET; A = ASA; C = ASA/MET combination).

are two key steps driving the metastatic process [50]. Intriguingly, ASA and MET acted both directly and indirectly on the tumor cells. On one hand, these drugs contained tumor mass growth and inhibited the migration of tumor cells from the primary malignant mass and the metastatic lymph nodes (direct action). On the other hand, they were shown to alleviate local vascular inflammation and, by doing so, reduce the deposition of circulating tumor cells (indirect action). Importantly, in the latter case, the drugs were not directly applied to the cancer cells, but they were rather applied to the endothelial cells, thus altering the vascular wall bioadhesive properties, possibly by decreasing the expression of adhesion molecules (e.g., ICAM, VCAM). So far, the reduction of cancer cell adhesion to the endothelium has been reported for ASA for breast cancer only [51]. Very importantly, here CRC cells derived from the primary tumor and from the lymph nodes of the same patient responded similarly to the ASA and MET treatments. This demonstrates the ability of ASA and MET to counteract CRC metastasis at different levels, thus encouraging the further development of ongoing clinical trials addressing the effects of ASA/MET combinations in CRC [23]. The presented results support the use of such a combination in MET-responsive patients, where the ASA/MET action appears to be additive or synergistic on tumor apoptosis, cell migration, and vascular adhesion, as also recently suggested [40]. While ASA worked in all tested patients, MET was only effective on three patients out of eight patients. Among the three MET-sensitive patients, one was diabetic, while the other two were neither diabetic nor insulin resistant. The significant variability observed among the different patients would highlight the importance of adopting personalized medicine approaches [39]. The most effective drug or drug combination could very well vary from patient to patient due to a number of factors, including the clinical history and the profile of genetic and epigenetic background of the patient [4,10,11]. Overall, patient-derived CRC cells represent a potent *in vitro* tool to generate simplified microversions of the original tumor, and the process could be easily scaled up towards high-throughput screening of multiple drugs, nanomedicines, and combinations thereof, aiming at promoting precision medicine.

Acknowledgements

This work was partially supported by Fondazione Compagnia di San Paolo through the project "Ligurian Alliance for Nanomedicine against Cancer", ID ROL 20608; the Italian Ministry for Foreign Affairs (MAECI) for the Italy-Serbia grant 2019 n. MAE0057596; ERA-NET on Translational Cancer Research (TRANSCAN) JTC 2013-056; and the Italian Association for Cancer Research (AIRC) grant IG 2014, Rif. 15468. The authors thank the Nikon Center and the Electron Microscopy Facility at Fondazione Istituto Italiano di Tecnologia for the support provided in imaging.

Declaration of Competing Interest

The authors declare no conflict of interest.

Appendix A. Supplementary data

Supplementary data to this article can be found online at https://doi.org/10.1016/j.tranon.2020.100760.

References

[1] RL Siegel, KD Miller, A Jemal, Cancer statistics, 2019, CA Cancer J. Clin. 69 (2019) 7–34.
[2] M Riihimaki, H Thomsen, K Sundquist, K Hemminki, Colorectal cancer patients: what do they die of? Frontline Gastroenterol 3 (2012) 143–149.
[3] M Riihimaki, A Hemminki, J Sundquist, K Hemminki, Patterns of metastasis in colon and rectal cancer, Sci. Rep. 6 (2016) 29765.

[4] DP Taylor, GJ Stoddard, RW Burt, MS Williams, JA Mitchell, PJ Haug, LA Cannon-Albright, How well does family history predict who will get colorectal cancer? Implications for cancer screening and counseling, Genet Med 13 (2011) 385–391.

[5] N Woolf, BE Pearson, PA Bondzie, RD Meyer, M Lavaei, AC Belkina, V Chitalia, N Rahimi, Targeting tumor multicellular aggregation through IGPR-1 inhibits colon cancer growth and improves chemotherapy, Oncogene 6 (2017), e378.

[6] Y Zhang, JT Fox, YU Park, G Elliott, G Rai, M Cai, S Sakamuru, R Huang, M Xia, K Lee, et al., A novel chemotherapeutic agent to treat tumors with DNA mismatch repair deficiencies, Cancer Res. 76 (2016) 4183–4191.

[7] D Spano, C Heck, P De Antonellis, G Christofori, M Zollo, Molecular networks that regulate cancer metastasis, Semin. Cancer Biol. 22 (2012) 234–249.

[8] AP Venook, D Niedzwiecki, HJ Lenz, F Innocenti, B Fruth, JA Meyerhardt, D Schrag, C Greene, BH O'Neil, JN Atkins, et al., Effect of first-line chemotherapy combined with cetuximab or bevacizumab on overall survival in patients with KRAS wild-type advanced or metastatic colorectal cancer: a randomized clinical trial, JAMA 317 (2017) 2392–2401.

[9] RL Anderson, T Balasas, J Callaghan, RC Coombes, J Evans, JA Hall, S Kinrade, D Jones, PS Jones, R Jones, et al., Cancer therapeutics, a framework for the development of effective anti-metastatic agents, Nat. Rev. Clin. Oncol. 16 (2019) 185–204.

[10] E Budinska, V Popovici, S Tejpar, G D'Ario, N Lapique, KO Sikora, AF Di Narzo, P Yan, JG Hodgson, S Weinrich, et al., Gene expression patterns unveil a new level of molecular heterogeneity in colorectal cancer, J. Pathol. 231 (2013) 63–76.

[11] L Losi, B Baisse, H Bouzourene, J Benhattar, Evolution of intratumoral genetic heterogeneity during colorectal cancer progression, Carcinogenesis 26 (2005) 916–922.

[12] HC Kwon, SY Oh, S Lee, SH Kim, HJ Kim, Bevacizumab plus infusional 5-fluorouracil, leucovorin and irinotecan for advanced colorectal cancer that progressed after oxaliplatin and irinotecan chemotherapy: a pilot study, World J. Gastroenterol. 13 (2007) 6231–6235.

[13] A Romera, S Peredpaya, Y Shparyk, I Bondarenko, G Mendonca Bariani, KC Abdalla, E Roca, F Franke, F Melo Cruz, A Ramesh, et al., Bevacizumab biosimilar BEVZ92 versus reference bevacizumab in combination with FOLFOX or FOLFIRI as first-line treatment for metastatic colorectal cancer: a multicentre, open-label, randomised controlled trial, Lancet Gastroenterol Hepatol 3 (2018) 845–855.

[14] G Giordano, A Remo, A Porras, M Pancione, Immune resistance and EGFR antagonists in colorectal cancer. Cancers (Basel), 11, 2019.

[15] A de Gramont, E Van Cutsem, HJ Schmoll, J Tabernero, S Clarke, MJ Moore, D Cunningham, TH Cartwright, JR Hecht, F Rivera, et al., Bevacizumab plus oxaliplatin-based chemotherapy as adjuvant treatment for colon cancer (AVANT): a phase 3 randomised controlled trial, Lancet Oncol. 13 (2012) 1225–1233.

[16] AB Chakravarthy, F Zhao, NJ Meropol, PJ Flynn, LI Wagner, J Sloan, RB Diasio, EP Mitchell, P Catalano, BJ Giantonio, et al., 3rd, Intergroup randomized phase III study of postoperative oxaliplatin, 5-fluorouracil, and leucovorin versus oxaliplatin, 5-fluorouracil, leucovorin, and bevacizumab for patients with stage II or III rectal cancer receiving preoperative chemoradiation: a trial of the ECOG-ACRIN Research Group (E5204), Oncologist (2019) 1–10.

[17] WA Hammond, A Swaika, K Mody, Pharmacologic resistance in colorectal cancer: a review, Ther Adv Med Oncol 8 (2016) 57–84.

[18] JR Vane, RM Botting, The mechanism of action of aspirin, Thromb. Res. 110 (2003) 255–258.

[19] B Viollet, B Guigas, N Sanz Garcia, J Leclerc, M Foretz, F Andreelli, Cellular and molecular mechanisms of metformin: an overview, Clin. Sci. (Lond.) 122 (2012) 253–270.

[20] W Yue, CS Yang, RS DiPaola, XL Tan, Repurposing of metformin and aspirin by targeting AMPK-mTOR and inflammation for pancreatic cancer prevention and treatment, Cancer Prev. Res. (Phila.) 7 (2014) 388–397.

[21] N Gronich, G Rennert, Beyond aspirin-cancer prevention with statins, metformin and bisphosphonates, Nat. Rev. Clin. Oncol. 10 (2013) 625–642.

[22] FV Din, A Valanciute, VP Houde, D Zibrova, KA Green, K Sakamoto, DR Alessi, MG Dunlop, Aspirin inhibits mTOR signaling, activates AMP-activated protein kinase, and induces autophagy in colorectal cancer cells, Gastroenterology 142 (2012) 1504–1515e1503.

[23] M Petrera, L Paleari, M Clavarezza, M Puntoni, S Caviglia, IM Briata, M Oppezzi, EM Mislej, B Stabuc, M Gnant, et al., The ASAMET trial: a randomized, phase II, double-blind, placebo-controlled, multicenter, 2 x 2 factorial biomarker study of tertiary prevention with low-dose aspirin and metformin in stage I-III colorectal cancer patients, BMC Cancer 18 (2018) 1210.

[24] PM Rothwell, M Wilson, CE Elwin, B Norrving, A Algra, CP Warlow, TW Meade, Long-term effect of aspirin on colorectal cancer incidence and mortality: 20-year follow-up of five randomised trials, Lancet 376 (2010) 1741–1750.

[25] CM Ulrich, J Bigler, JD Potter, Non-steroidal anti-inflammatory drugs for cancer prevention: promise, perils and pharmacogenetics, Nat. Rev. Cancer 6 (2006) 130–140.

[26] S Umezawa, T Higurashi, Y Komiya, J Arimoto, N Horita, T Kaneko, M Iwasaki, H Nakagama, A Nakajima, Chemoprevention of colorectal cancer: past, present, and future, Cancer Sci. 110 (2019) 3018–3026.

[27] N Joharatnam-Hogan, F Cafferty, R Hubner, D Swinson, S Sothi, K Gupta, S Falk, K Patel, N Warner, V Kunene, et al., G. Add-Aspirin Trial Management, Aspirin as an adjuvant treatment for cancer: feasibility results from the Add-Aspirin randomised trial, Lancet Gastroenterol Hepatol 4 (2019) 854–862.

[28] A Decensi, M Puntoni, P Goodwin, M Cazzaniga, A Gennari, B Bonanni, S Gandini, Metformin and cancer risk in diabetic patients: a systematic review and meta-analysis, Cancer Prev. Res. (Phila.) 3 (2010) 1451–1461.

[29] P Saraei, I Asadi, MA Kakar, N Moradi-Kor, The beneficial effects of metformin on cancer prevention and therapy: a comprehensive review of recent advances, Cancer Manag. Res. 11 (2019) 3295–3313.

[30] L Paleari, J Burhenne, J Weiss, S Foersch, W Roth, A Parodi, M Gnant, T Bachleitner-Hofmann, D Scherer, CM Ulrich, et al., High accumulation of metformin in colonic tissue of subjects with diabetes or the metabolic syndrome, Gastroenterology 154 (2018) 1543–1545.

[31] M Petrera, L Paleari, M Puntoni, S Caviglia, M Clavarezza, P Romagnolli, M Gnant, WE Haefeli, W Roth, D Scherer, et al., ASAMET: a randomized, 2×2 biomarker prevention trial of low-dose aspirin and metformin in colorectal cancer, J. Clin. Oncol. 35 (2017).

[32] H Sorbye, CH Kohne, DJ Sargent, B Glimelius, Patient characteristics and stratification in medical treatment studies for metastatic colorectal cancer: a proposal for standardization of patient characteristic reporting and stratification, Ann. Oncol. 18 (2007) 1666–1672.

[33] NH Tran, LL Cavalcante, SJ Lubner, DL Mulkerin, NK LoConte, L Clipson, KA Matkowskyj, DA Deming, Precision medicine in colorectal cancer: the molecular profile alters treatment strategies, Ther Adv Med Oncol 7 (2015) 252–262.

[34] TEL Voyer, ER Sigurdson, AL Hanlon, RJ Mayer, JS Macdonald, PJ Catalano, DG Haller, Colon cancer survival is associated with increasing number of lymph nodes analyzed: a secondary survey of Intergroup Trial INT-0089, J. Clin. Oncol. 21 (2003) 2912–2919.

[35] AC Berger, ER Sigurdson, T LeVoyer, A Hanlon, RJ Mayer, JS Macdonald, PJ Catalano, DG Haller, Colon cancer survival is associated with decreasing ratio of metastatic to examined lymph nodes, J. Clin. Oncol. 23 (2005) 8706–8712.

[36] X Xu, MC Farach-Carson, X Jia, Three-dimensional in vitro tumor models for cancer research and drug evaluation, Biotechnol. Adv. 32 (2014) 1256–1268.

[37] G Palazzolo, N Broguiere, O Cenciarelli, H Dermutz, M Zenobi-Wong, Ultrasoft alginate hydrogels support long-term three-dimensional functional neuronal networks, Tissue Eng Part A 21 (2015) 2177–2185.

[38] C Manneschi, RC Pereira, G Marinaro, A Bosca, M Francardi, P Decuzzi, A microfluidic platform with permeable walls for the analysis of vascular and extravascular mass transport, Microfluid. Nanofluid. 20 (2016) 113.

[39] C Molinari, G Marisi, A Passardi, L Matteucci, G De Maio, P Ulivi, Heterogeneity in colorectal cancer: a challenge for personalized medicine? Int. J. Mol. Sci. 19 (2018).

[40] A De Monte, D Brunetti, L Cattin, F Lavanda, E Naibo, M Malagoli, G Stanta, S Bonin, Metformin and aspirin treatment could lead to an improved survival rate for Type 2 diabetic patients with stage II and III colorectal adenocarcinoma relative to non-diabetic patients, Mol Clin Oncol 8 (2018) 504–512.

[41] PR Prasetyanti, JP Medema, Intra-tumor heterogeneity from a cancer stem cell perspective, Mol. Cancer 16 (2017) 41.

[42] R Gangemi, L Paleari, AM Orengo, A Cesario, L Chessa, S Ferrini, P Russo, Cancer stem cells: a new paradigm for understanding tumor growth and progression and drug resistance, Curr. Med. Chem. 16 (2009) 1688–1703.

[43] H Mollica, A Coclite, ME Miali, RC Pereira, L Paleari, C Manneschi, A DeCensi, P Decuzzi, Deciphering the relative contribution of vascular inflammation and blood rheology in metastatic spreading, Biomicrofluidics 12 (2018), 042205.

[44] AL Palange, D Di Mascolo, C Carallo, A Gnasso, P Decuzzi, Lipid-polymer nanoparticles encapsulating curcumin for modulating the vascular deposition of breast cancer cells, Nanomedicine 10 (2014) 991–1002.

[45] H Mollica, R Palomba, R Primavera, P Decuzzi, Two-channel compartmentalized microfluidic chip for real-time monitoring of the metastatic cascade, ACS Biomaterials Science & Engineering 5 (2019) 4834–4843.

[46] MS Singh, M Goldsmith, K Thakur, S Chatterjee, D Landesman-Milo, T Levy, LA Kunz-Schughart, Y Barenholz, D Peer, An ovarian spheroid based tumor model that represents vascularized tumors and enables the investigation of nanomedicine therapeutics, Nanoscale 12 (2020) 1894–1903.

[47] Z Zhang, YC Chen, S Urs, L Chen, DM Simeone, E Yoon, Scalable multiplexed drug-combination screening platforms using 3D microtumor model for precision medicine, Small 14 (2018), e1703617.

[48] J Kondo, T Ekawa, H Endo, K Yamazaki, N Tanaka, Y Kukita, H Okuyama, J Okami, F Imamura, M Ohue, et al., High-throughput screening in colorectal cancer tissue-originated spheroids, Cancer Sci. 110 (2019) 345–355.

[49] E Brauchle, J Kasper, R Daum, N Schierbaum, C Falch, A Kirschniak, TE Schaffer, K Schenke-Layland, Biomechanical and biomolecular characterization of extracellular matrix structures in human colon carcinomas, Matrix Biol. 68-69 (2018) 180–193.

[50] DR Welch, DR Hurst, Defining the hallmarks of metastasis, Cancer Res. 79 (2019) 3011–3027.

[51] E Bischofs, D Lubs, F Fritzsche, AS Meyer, T Bruckner, C Sohn, MH Eichbaum, In vitro blockade of adhesion of breast cancer cells to endothelial cells using anti-inflammatory drugs, Anticancer Res. 32 (2012) 767–771.